Optical cleaning owing to the bulk photovoltaic effect

B. Sturman,[1] M. Kösters,[2] D. Haertle,[2] C. Becher,[2] and K. Buse[2]
[1]*Institute of Automation and Electrometry, 630090 Novosibirsk, Russia*
[2]*Institute of Physics, University of Bonn, Wegelerstraße 8, D-53115 Bonn, Germany*
(Received 31 August 2009; revised manuscript received 18 November 2009; published 18 December 2009)

It is shown within the conventional photovoltaic charge-transport model that photoexcitable electrons, localized at deep impurity levels, can be effectively removed by light from the exposed area at sufficiently high temperatures. This allows to modify strongly the absorption and photoelectric properties of the material and, in particular, to suppress "optical damage" in $LiNbO_3$ and $LiTaO_3$ crystals. This optical cleaning method is applicable to numerous pyro- and piezo-electric optical materials. It employs the photovoltaic drift of electrons and ionic charge compensation at elevated temperatures. The physics of the optical cleaning is very rich; it has strong links to nonlinear dynamics and offers important handles for improvement of the cleaning performance. The use of properly moving light beams leads, e.g., to a strong enhancement of the cleaning rate and allows to reduce the electron concentration by several orders of magnitude. The theoretical predictions are supported by the data of our cleaning experiments with $LiNbO_3$ crystals. In particular, the intensity threshold of optical damage is increased by three orders of magnitude.

DOI: 10.1103/PhysRevB.80.245319 PACS number(s): 42.65.Hw, 42.50.Gy, 78.20.Bh

I. INTRODUCTION

The bulk photovoltaic (PV) effect is the generation of continuous electric currents by light in the absence of electric and magnetic fields and spatial gradients.[1] This effect, discovered in 1974,[2] can occur in any noncentrosymmetric medium, characterized generally by a third-rank PV tensor, and is known in numerous crystals of the pyro- and piezo-electric symmetry, including the ferroelectrics $LiNbO_3$, $LiTaO_3$, $KNbO_3$, $BaTiO_3$, and the cubic semiconductors GaAs, CdTe, and InP.[1] In crystals of the pyroelectric symmetry, the PV currents flow typically along the polar axis. These currents are linear in the light intensity and significant already in the low-intensity range. They lead, in particular, to the buildup of permanent electric fields reaching (10^3-10^5) V/cm in the steady state when balanced by the Ohmic currents. In wide-gap optical materials, including the mentioned ferroelectrics, the photovoltaic effect is typically of extrinsic origin.[1,2] It accompanies electron transitions from localized states in the forbidden gap either to the conduction or to the valence band.

Lithium niobate occupies a special place among the polar optical materials. On the one hand, it has a potential to become the "silicon of photonics." The reason is a unique combination of important properties: the ease of fabrication and robustness, transparency in the visible-to-infrared spectral ranges, sensitization by doping, excellent electro-optic and nonlinear-optical characteristics, and the ability to shape domain structures for quasiphase-matching.[3–7] On the other hand, the PV effect leads here (as in $LiTaO_3$ crystals) to strong optical manifestations owing to the generation of high electric fields, up to 10^5 V/cm, causing large refractive index changes via the linear electro-optic effect.[1,2,8] While these index changes are useful for some applications, they are the main obstacle for the employment of $LiNbO_3$ in optics because of a strong deterioration of light beams known as optical damage.[3,9,10] This optical damage occurs even in nominally undoped crystals because of the presence of remnant ions of Fe.

It is noteworthy that a relatively small fraction of the total amount of electrons—the photoexcitable electrons—determines greatly the photoelectric properties of numerous optical materials in the visible-to-infrared spectral ranges. The energy position and occupancy of deep impurity levels are determined by intentionally doped or remnant impurities and by chemical treatments such as oxidization and reduction. Shaping of the localized electronic states is a high-priority task for numerous optical applications.[11–14]

Recently, we have presented a method for the removal of the photoexcitable electrons from the exposed region in photovoltaic crystals, the method of *optical cleaning*.[15] It makes use of the main ingredient of the PV effect—the presence of a light-induced directional electron flow—and, additionally, of sufficiently high temperatures to activate the ionic conductivity and to prevent the blocking effect of arising electric fields. An experimental proof of the principle has been given for $LiNbO_3$ crystals and some prominent expected features of the effect were mentioned.

The present study goes far beyond Ref. 15. It gives a conclusive analysis of the optical cleaning effect within a general charge-transport model and reveals the big potential of the cleaning method. Our theoretical considerations show that the optical cleaning is a massive and physically rich effect. This includes the accessibility of qualitatively different cleaning regimes, sharp dependences on the variable experimental and key material parameters, and nontrivial optimization issues. It is proven that a (3–4) orders-of-magnitude decrease in the electron concentration can occur exponentially, i.e., extremely fast, when using properly shaped moving light beams. To the best of our knowledge, no similar phenomena have been known in solid-state and optical physics.

Our theoretical considerations combine the powerful analytical method of characteristics[16] (known also as transition from the Euler to Lagrange variables) with direct numerical simulations. They show surprisingly strong links with hydrodynamic models describing linear and nonlinear waves.[17,18]

Last, we compare the theoretical predictions with available experimental data.

It is necessary to underline that the photovoltaic coefficients of $LiNbO_3$ crystals are not much different from those typical for many other noncentrosymmetric optical materials.[1] Our model considerations are thus of relevance for a broad range of materials. However, lithium niobate is the most important and investigated optical material. This is why we employ exemplarily its photo-electric and charge-transport properties when modeling the optical cleaning. In particular, we make use of the knowledge accumulated in the studies of the thermal fixing phenomenon in $LiNbO_3$ crystals: formation of permanent ionic gratings during heating of the sample.[19–21]

II. PHYSICAL BACKGROUND

We assume that photoexcitable electrons are localized initially at deep centers near the Fermi level. The total concentration of the electrons available is denoted as N_e; its background (initial) value N_e^0 is expected to be considerably smaller than the total concentration of the centers N_Σ =const. In lithium niobate, the filled centers are usually attributed to Fe^{2+} (or Cu^+) ions, while the empty centers are in the Fe^{3+} (or Cu^{2+}) valence states.[7,22] The filled and empty centers act as sources and traps, respectively, for the photoexcited electrons.

Photo excitation of electrons from the deep centers to the conduction-band results in an electronic current owing to the photovoltaic effect and also owing to the drift and diffusion of free electrons. The corresponding relation for the electronic current density j_e can be written as

$$j_e = -e\beta N_e I + e\mu_e\left(n_e E + \frac{k_B T}{e}\frac{\partial n_e}{\partial z}\right), \tag{1}$$

where $I=I(z,t)$ is the light intensity, $E=E(z,t)$ is the electric field, $n_e=n_e(z,t)$ and μ_e are the concentration and mobility of the photoexcited (free) electrons, β is the photovoltaic constant, z and t are the coordinate and the time, e is the elementary charge, k_B is the Boltzmann constant, and T is the absolute temperature. The photovoltaic current, given by the first term of Eq. (1), can be viewed as a light-induced drift of electrons in the absence of an electric field.

The free electron concentration n_e can be expressed by N_e and I,

$$n_e = \frac{sN_e I}{\hbar\omega}\tau_e, \tag{2}$$

where s is the known light-absorption cross-section (e.g., $s \approx 5\times 10^{-18}$ cm^2 at 477 nm[23]), $\hbar\omega$ is the energy of a light quantum and τ_e is the lifetime of the free electrons. Since the lifetime τ_e is short, the quasiequilibrium between the photoexcitation and recombination processes occurs practically instantaneously, and the concentration of the free electrons is relatively small, $n_e \ll N_e$. It is necessary to keep in mind that the lifetime τ_e depends generally on N_e, but this dependence becomes important only when the trap concentration $N_\Sigma - N_e$ is sufficiently small.

The photovoltaic constant β is conventionally expressed by the measurable photovoltaic shift l_{pv} of an electron per absorbed photon, $\beta = sl_{pv}/\hbar\omega$; typically $l_{pv} \approx 1$ Å in lithium niobate.[1,2] The photoconductivity is given by $\sigma_{ph} = (es/\hbar\omega)\mu_e\tau_e N_e I$; the mobility-lifetime product $\mu_e\tau_e$ is also a measurable material parameter. Its anomalously small value, $\mu_e\tau_e \approx (10^{-13}-10^{-12})$ cm^2/V,[1] is the reason for the large photovoltaic field, $E_{pv} \equiv l_{pv}/\mu_e\tau_e \approx (10^4-10^5)$ V/cm, at room temperature.

The photovoltaic length l_{pv} grows slightly with increasing temperature in the actual range $T=(20-180)$ °C, while the photoconductivity σ_{ph} shows a weak thermoactivation dependence with an activation energy $\varepsilon_e \simeq 0.15$ eV.[1]

The diffusion contribution in Eq. (1) is negligible compared to the photovoltaic one unless the spatial profile of $N_e(z)$ becomes steep on the submicrometer scale. Retaining of this contribution, as we will see, is necessary only to prevent breaking of the electron profile if it happens without a diffusion smoothing. A similar status of diffusion effects is known in the theory of nonlinear waves.[17,18]

The second type of mobile charge carriers, which is necessary for the optical cleaning, is provided by optically passive ions. Typically, they can be identified with hydrogen ions H^+ in lithium niobate for $T \lesssim 180$ °C.[21,24,25] The hydrogen concentration $N_i=N_i(z,t)$ exceeds usually 10^{18} cm^{-3}. The density of the ionic current is generally

$$j_i = e\mu_i\left(N_i E - \frac{k_B T}{e}\frac{\partial N_i}{\partial z}\right), \tag{3}$$

where μ_i is the ion mobility. The ionic conductivity is given by $\sigma_i = e\mu_i N_i$. The combination $D_i = \mu_i k_B T/e$ is the diffusion coefficient for the ions. It is thermally activated and can be conventionally represented as $D_i = D_i^0 \exp(-\varepsilon_i/k_B T)$; the activation energy ε_i is typically in the range (1.1–1.2) eV for H^+ ions.[21,26] Data on the pre-exponent D_i^0 are also available in the literature.[25,27] The diffusion component of the ionic current, given by the second term in Eq. (3), can be neglected; it plays no significant role compared to the electronic diffusion component.

The set of coupled equations for $N_{e,i}$ and E consists of the continuity equations

$$\frac{\partial N_e}{\partial t} = +\frac{1}{e}\frac{\partial j_e}{\partial z}, \tag{4}$$

$$\frac{\partial N_i}{\partial t} = -\frac{1}{e}\frac{\partial j_i}{\partial z}, \tag{5}$$

and the Poisson equation

$$\frac{\partial E}{\partial z} = \frac{e}{\epsilon\epsilon_0}(N_i - N_e - N_i^0 + N_e^0), \tag{6}$$

where $\epsilon\epsilon_0$ is the static dielectric constant, and $N_{e,i}^0$=const are the background concentrations of electrons and ions. The concentrations N_e and N_i are coupled to each other only via the field-dependent contributions to $j_{e,i}$.

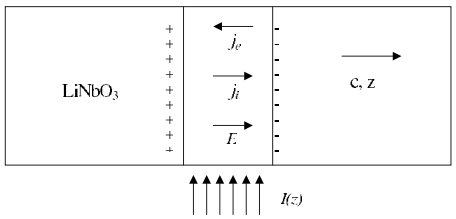

FIG. 1. Scheme of the electrical equilibrium for a square-wave-shaped light intensity profile $I(z)$. The electronic current is the sum of the photovoltaic and drift currents, $j_e=j_{pv}+\sigma_{ph}E$, while the ionic current is solely due to the drift, $j_i=\sigma_i E$.

III. AN ELEMENTARY CONSIDERATION

Let the electron and ion concentrations be initially spatially uniform, $N_{e,i}(z,0)=N_{e,i}^0$, and the crystal be illuminated by a narrow square-wave-shaped light strip with $I=I_0$ =const and $\sigma_{ph}=\sigma_{ph}^0$=const inside the illuminated region and zero outside it, see Fig. 1. The photovoltaic current $j_{pv}=-e\beta N_e^0 I_0$ induces opposite charges at the borders of the region and a uniform electric field inside of it. After a short time of the order of the dielectric relaxation time $t_d=\epsilon\epsilon_0/(\sigma_{ph}^0+\sigma_i^0)$, the system reaches electrical equilibrium where the total current is practically zero, $j_e+j_i=0$, and the field is $E=E_{pv}/(1+\sigma_i^0/\sigma_{ph}^0)$. The electronic and ionic currents are nonzero and opposite in this equilibrium, $j_{e,i}=\mp j_{pv}/(1+\sigma_{ph}^0/\sigma_i^0)$. The maximum absolute values of these currents occur for $\sigma_i^0 \gg \sigma_{ph}^0$, when $E \ll E_{pv}$ and the blocking effect of the field E is negligible. In the opposite limit, $\sigma_i^0/\sigma_{ph}^0 \to 0$, which can be approached for weaker heating, we have $j_e \to 0$. Here the light-induced field blocks the photovoltaic current completely.

Thus, it is evident that the electrical equilibrium is far from a true equilibrium for $\sigma_i^0 \gg \sigma_{ph}^0$. It is accompanied by almost the same fluxes of electrons and positive ions to the "minus" border of the illuminated region where accumulation of these carriers takes place. Ultimately, all electrons are expected to be removed from the illuminated region, if the concentration of the compensating passive ions is big enough to ensure charge compensation, i.e., $N_i^0 \gg N_e^0$.

The characteristic time of the cleaning process t_0 can be estimated if we divide the width of the illuminated region (let it be z_0) by the velocity of the photovoltaic drift $v_0=j_{pv}/eN_e^0=sl_{pv}I_0/\hbar\omega$. We have thus $t_0=z_0\hbar\omega/sI_0l_{pv}$. It is about a few hours for $z_0=1$ mm and $I_0=10^2$ W/cm^2, which is much longer than the dielectric relaxation time t_d. Thus, the electric equilibrium has to be treated as a quasiequilibrium.

It is worth mentioning that the ratio of the characteristic times t_0/t_d can be represented as

$$\frac{t_0}{t_d} \approx \frac{E_q}{E_{pv}}\left(1+\frac{\sigma_i^0}{\sigma_{ph}^0}\right), \tag{7}$$

where $E_q \approx ez_0N_e^0/\epsilon\epsilon_0$ is the so-called charge saturation field.[8] The notion of the quasiequilibrium works thus perfectly well for $E_{pv} \ll E_q$ and $\sigma_{ph}^0 \ll \sigma_i^0$, and it is closely related to the absence of electronic charge saturation.

While the square-shaped light strip is convenient for elementary considerations and estimates, it is inconvenient for practical purposes. Below we consider in detail the cleaning process for one-dimensional Gaussian light beams.

IV. THEORY OF THE CLEANING PROCESS

In what follows we employ a moving Gaussian intensity profile

$$I=I_0\exp[-(z-vt)^2/z_0^2], \tag{8}$$

where z_0 is the Gaussian width and v is the beam velocity. Optimization of v, as we show below, provides an exponential enhancement of the cleaning rate.

To simplify our considerations, we transfer to a coordinate frame moving with velocity v and normalize the coordinate and time to z_0 and $t_0=z_0\hbar\omega/sI_0l_{pv}$, respectively. Explicitly, the new spatiotemporal variables, marked with a hat, are:

$$\hat{z}=(z-vt)/z_0, \quad \hat{t}=t/t_0. \tag{9}$$

Next, we introduce the normalized electron concentration $\rho=N_e/N_e^0$ and the normalized intensity $f=I/I_0$. The latter depends solely on $\hat{z}$, $f=\exp(-\hat{z}^2)$.

Methodically, we will proceed step by step from the simplest to more complicated cases.

A. Basic model of cleaning

Let us suppose that $\sigma_i \gg \sigma_e$ and $N_i \gg N_e$, i.e., that the negative blocking effect of the light-induced field can be neglected and the electrons are driven solely by the photovoltaic effect. This situation is ultimately favorable for the optical cleaning.

Keeping only the first term in Eq. (1), we have then from Eq. (4) in the normalized variables:

$$\frac{\partial\rho}{\partial\hat{t}}+\frac{\partial u\rho}{\partial\hat{z}}=0, \tag{10}$$

where $u=u(\hat{z})=f(\hat{z})-r$ is the effective velocity profile, $r=v/v_0$ is a variable constant, and $v_0=sl_{pv}I_0/\hbar\omega$ is the characteristic velocity of the photovoltaic drift. This first-order partial differential equation must be solved with the initial condition $\rho(\hat{z},0)=1$.

1. Solution method

Physically, the above continuity equation is equivalent to that describing the following classical kinematic problem: initially, at $\hat{t}=0$, noninteracting individual particles are distributed uniformly along the $\hat{z}$ axis. Then each particle moves with the $\hat{z}$-dependent velocity $u(\hat{z})$ starting from its initial position. What is the concentration of the particles $\rho(\hat{z},\hat{t})$ for $\hat{t}>0$?

The general solution of this problem is also known. It can be expressed in terms of trajectories of the individual particles having different initial coordinates.[17,18] Mathematically, the calculation procedure is closely related to the method of characteristics.[16] Let $\hat{z}(\hat{t})$ obey the motion equation

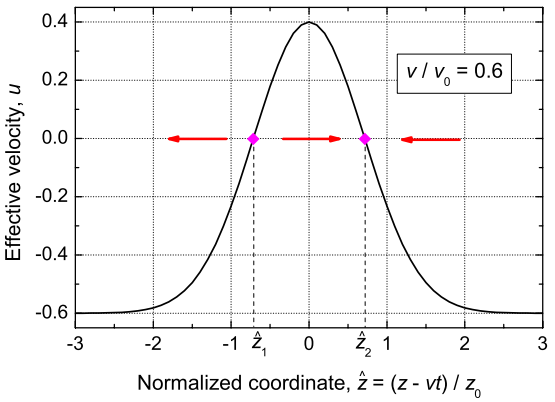

FIG. 2. (Color online) Dependence $u(\hat{z})$ for $r=v/v_0=0.6$. The dots show the zero points of u, while the arrows show the directions of motion of electrons in different regions of $\hat{z}$.

$$\frac{d\hat{z}}{d\hat{t}} = u(\hat{z}), \tag{11}$$

with an initial condition $\hat{z}(0)=\xi$, where ξ is a variable parameter. Solution of this ordinary differential equation gives a family of trajectories (characteristics), i.e., a function $\hat{z}=\hat{z}(\hat{t},\xi)$. It can be viewed also as the transition from the set $\{\hat{z},\hat{t}\}$ (the Euler variables) to the set $\{\xi,\hat{t}\}$ (the Lagrange variables).[18] One can check straightforwardly that Eq. (10), rewritten in the Lagrange variables, reads $\partial(\rho u)/\partial\hat{t}=0$, so that the product ρu remains constant along each characteristic, and the necessary general solution for ρ is

$$\rho(\hat{z},\hat{t}) = \frac{u(\xi)}{u(\hat{z})} \equiv \frac{u(\xi(\hat{z},\hat{t}))}{u(\hat{z})}. \tag{12}$$

The dependences $\hat{z}(\xi,t)$ and $\xi(\hat{z},t)$ cannot be calculated analytically for the Gaussian intensity profile. However, the motion Eq. (11) can be easily solved numerically providing the necessary concentration profiles. For any particular value of $\hat{t}$ it is sufficient to express ξ by $\hat{z}$ in order to plot the corresponding concentration profile $\rho(\hat{z})$.

It is important that the effective velocity profile $u(\hat{z})=\exp(-\hat{z}^2)-r$ with $r=v/v_0$ has two zero (fixed) points $\hat{z}_{1,2}=\mp\sqrt{\ln(1/r)}$ for $0<r<1$, as it is illustrated by Fig. 2. The particles standing initially exactly at $\hat{z}_{1,2}$ remain fixed, the particles standing in the vicinity of the left fixed point $\hat{z}_1$ diverge from it, and the particles standing in the vicinity of the right fixed point $\hat{z}_2$ converge on it. One can suggest that the concentration $N(\hat{z})$ is minimal and maximal just at these fixed points.

Mathematically, the mentioned feature means that $\hat{z}=\xi$ at the fixed points, so we have here a 0/0 uncertainty in Eq. (12). This uncertainty can be resolved using Eq. (11) to calculate analytically the time dependence of $\rho=N_e/N_e^0$ at the fixed points providing the result

$$\rho(\hat{z}_{1,2},\hat{t}) = \exp(\gamma_{1,2}\hat{t}), \tag{13}$$

where the rate constants γ_1 and γ_2 are opposite to each other and given by

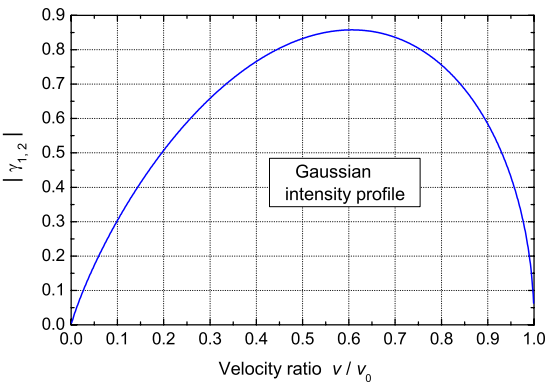

FIG. 3. (Color online) The absolute value of the rate coefficient $|\gamma_{1,2}|$ versus the velocity ratio v/v_0 for the Gaussian cleaning beam.

$$\gamma_{1,2} = \mp (2v/v_0)\sqrt{\ln(v_0/v)}. \tag{14}$$

Thus, the electron concentration is decreasing and increasing *exponentially*, i.e., extremely fast, at the fixed points $\hat{z}_1$ and $\hat{z}_2$, respectively.

As a function of v/v_0, the absolute value $|\gamma_{1,2}|$ has a maximum, $|\gamma_{1,2}|_{max}\simeq 0.86$, at $v/v_0\simeq 0.6$, see Fig. 3. This velocity ratio is thus the optimum for the cleaning purposes. Physically, this optimal condition corresponds to the largest value of the derivative $du/d\hat{z}$ taken at the fixed points. For $v=0$ and $v=v_0$, when the fixed points vanish, the increment turns to zero.

It is useful to rewrite the exponent $\gamma_{1,2}\hat{t}$ in the form,

$$\gamma_{1,2}\hat{t} = -(v_0 t/I_0)(dI/dz)_{1,2}, \tag{15}$$

where the spatial derivative is taken at the fixed points. One can see explicitly that the absolute value of $\gamma_{1,2}$ grows with decreasing Gaussian width z_0. The steeper the beam profile, the larger is the cleaning rate.

2. Different cleaning regimes

We consider first the simplest regime which employs a standing Gaussian light beam, $v=0$. The solid lines in Fig. 4 show concentration profiles calculated numerically by the method of characteristics for four different values of the cleaning time t. The effect of cleaning is already strongly

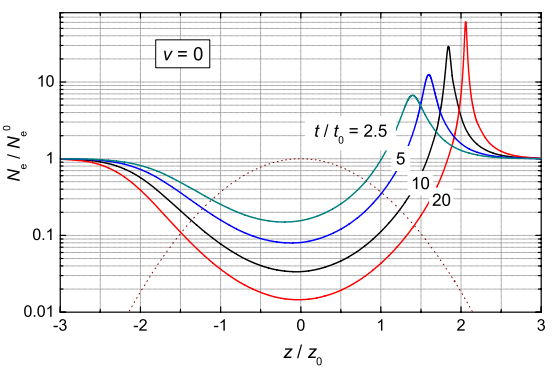

FIG. 4. (Color online) The concentration profile for $v=0$ and four values of the normalized time t/t_0 within the basic model. The dotted line is the normalized intensity profile I/I_0.

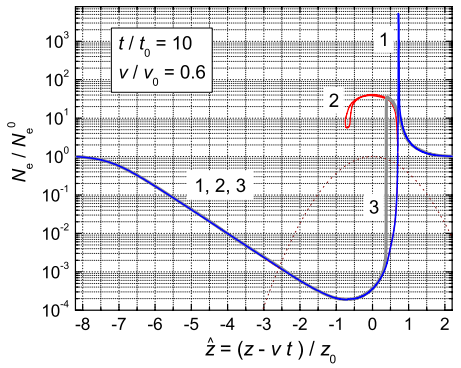

FIG. 5. (Color online) The normalized profile $N_e(\hat{z})/N_e^0$ for $t/t_0=10$ and $v/v_0=0.6$. For line 1, the impact of the light-induced field is neglected, i.e., parameters a,b,c given by Eq. (18) are set to be zero. Line 2 accounts for the effect of a space-charge field at $a,b,c=0.01$ but ignores diffusion. Line 3 is plotted for $a,b,c=0.01$ and electron diffusion is taken into account. Lines 2 and 3 coincide with line 1 except for the peak region of N_e. The dotted line shows the normalized intensity profile.

pronounced in this case. We have a broad concentration minimum (the cleaned area) and a relatively narrow concentration peak at the right tail of the cleaning beam. As expected, the decrease in ρ_{max} and the increase in ρ_{min} occur nonexponentially in time. For $t/t_0=20$, the value of ρ_{min} is of the order of 10^{-2}.

Now we turn to the cleaning regimes which make use of moving Gaussian beams and consider first the case $v/v_0=0.6$, which is expected to give the maximum cleaning rate. Line 1 in Fig. 5 shows the concentration profile calculated numerically for $\hat{t}=10$. The positions of the minimum and maximum correspond exactly to the above analytical results. The broad cleaned area to the left of the very sharp peak is expanding in time by shifting to the left in the moving coordinate frame. This corresponds to the physical picture of bulldozering of the electrons by the moving light beam in the standing coordinate frame. Note that (i) the time dependence of ρ is not exponential for $\hat{z}\neq\hat{z}_{1,2}$, and (ii) the spatial dependence $\rho(\hat{z})$ is almost linear within the wide range $-7\lesssim\hat{z}\lesssim -1$ in the logarithmic scale used.

The impact of the velocity ratio v/v_0 on the ratio N_e^{min}/N_e^0 is illustrated also by Fig. 6. Strong enhancement of the cleaning performance by means of optimization of v/v_0 is evi-

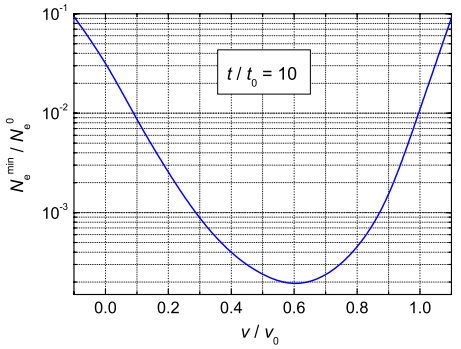

FIG. 6. (Color online) The ratio $N_e^{min}/N_e^0=\rho_{min}$ versus v/v_0 for $t/t_0=10$ within the basic model.

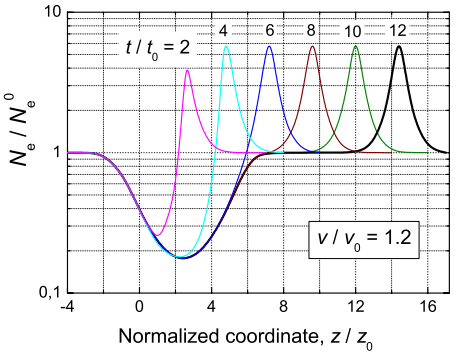

FIG. 7. (Color online) Normalized concentration profiles in the standing coordinate frame for $v/v_0=1.2$ and six values of the cleaning time, $t/t_0=2$, 4, 6, 8, 10, and 12.

dent. With increasing t/t_0 it becomes even more pronounced.

It is worth mentioning that the cleaning scenario is changing qualitatively for the supercritical beam velocities $v>v_0$. The light beam becomes eventually separated from the cleaned area and bulldozering only a time-constant amount of electrons. This scenario is illustrated by Fig. 7. The cleaning performance drops down strongly in the supercritical case.

As follows from the above analytical considerations, the cleaning performance can be further improved using asymmetric moving light beams with relatively sharp trailing edges, flat tops, and smooth leading edges. Equations (13) and (15) are still valid in this case, however, we have $\gamma_2 \ll|\gamma_1|$. The large derivative $dI/d\hat{z}$ at the trailing edge for such a beam ensures a large rate of the exponential decrease in $N_e^{min}(\hat{z})$. The presence of the flat top ensures an enlargement of the cleaned area and the spatial separation of the points of minimum and maximum of $N_e(\hat{z})$. The small derivative at the leading edge provides broadening of the concentration peak in front of the cleaning beam.

Figure 8 gives an example of the influence of the beam asymmetry. The solid line 1, taken as a reference point, exhibits the known concentration profile for the Gaussian beam (the dotted line 1′), $t/t_0=10$, and $v/v_0=0.6$. The solid line 2

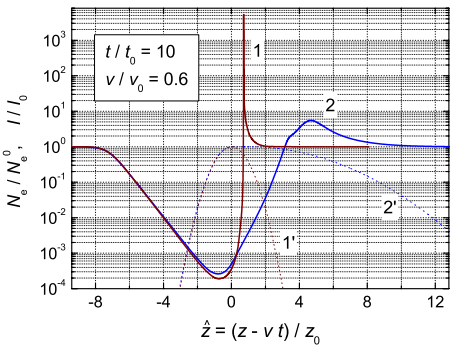

FIG. 8. (Color online) Influence of asymmetry of the cleaning light beam on the cleaning performance. The dotted lines 1′ and 2′ show the symmetric and asymmetric beam profiles, respectively. The width parameter of both trailing edges is z_0, $t/t_0=10$, and $v/v_0=0.6$. The solid lines 1 and 2 show the corresponding concentration profiles.

shows the concentration profile for a moving asymmetric beam (the dotted line 2′) whose trailing edge is close to that of the Gaussian beam, while the top is flat and the leading edge is relatively smooth. The other cleaning parameters are the same. The concentration profiles are almost the same within a broad region $\hat{z} \lesssim 1$. At the same time, the concentration peak is strongly suppressed and shifted to the right in the asymmetric case. The suppression factor corresponds to a fivefold decrease of the derivative dI/dz at the fixed point z_2.

Note lastly that the presence of a weak polluting background illumination of the intensity $I_b \ll I_0$, caused, e.g., by slight scattering of the cleaning beam, results merely in a renormalization of the beam velocity, $v \to v + \delta v$ with $\delta v = (I_b/I_0)v_0 \ll v_0$, within our scheme.

B. Impact of the light-induced field

As we have seen in the previous subsection, the peak of the electron concentration becomes very high already for not very large normalized times t/t_0, which is indeed a direct consequence of the bulldozering effect. One can expect that the approximation $\sigma_{ph} \ll \sigma_i$ breaks here even for the relatively small background photoconductivity, $\sigma_{ph}^0 \ll \sigma_i^0$. Just here, in the narrow peak region, one can expect a serious modification of our theory. As for the broad cleaned area behind the peak, where $N_e \lesssim N_e^0$ and $\sigma_{ph} \lesssim \sigma_{ph}^0$, the above concentration profiles are unlikely to be subjected to strong changes.

To analyze the influence of the light-induced field E, we adopt a local-equilibrium approximation. It makes use of the fact that the field-relaxation time t_d is much shorter than the photovoltaic-drift time t_0. Therefore, we can set $j_e + j_i \simeq 0$ to express E by $N_{e,i}$ in the leading approximation. Simultaneously, we obtain the equality $N_e + N_i \simeq N_e^0 + N_i^0$, which means an almost complete charge compensation, within the same approximation. The above two relations enable us to express algebraically E and N_i by N_e in Eq. (4) and we come again to a single equation for the normalized electron concentration $\rho = N_e/N_e^0$.

Neglecting the diffusion contributions to the electric current densities $j_{e,i}$, we present this single partial differential equation in the form

$$\frac{\partial \rho}{\partial \hat{t}} + u\frac{\partial \rho}{\partial \hat{z}} = g, \tag{16}$$

which looks structurally similar to that of Eq. (10). The difference is that the effective velocity u and driving force g are now functions of not only $\hat{z}$ but also of ρ: $u = u(\hat{z}, \rho)$ and $g = g(\hat{z}, \rho)$. Mathematically, it is a quasilinear equation, which is *linear* in the spatiotemporal derivatives of ρ but *nonlinear* in ρ.[16,18]

To proceed to particular expressions for $u(\hat{z}, \rho)$ and $g(\hat{z}, \rho)$, we must take into account that the electron concentration N_e cannot exceed the total concentration of deep centers N_Σ within our model, which corresponds to the relation $\tau_e^{-1} \propto N_\Sigma - N_e$. The final expressions for u and g are:

$$u = f\frac{(1 - c\rho)^2(1 + b\rho)^2 + af\rho^2(b - c - 2bc\rho)}{[af\rho + (1 - c\rho)(1 + b\rho)]^2} - r,$$

$$g = 2\hat{z}f\rho\frac{(1 - c\rho)^2(1 + b\rho)^2}{[af\rho + (1 - c\rho)(1 + b\rho)]^2}, \tag{17}$$

where

$$a = \sigma_{ph}^0/\sigma_i^0, \quad b = N_e^0/N_i^0, \quad c = N_e^0/N_\Sigma \tag{18}$$

are three dimensionless input parameters characterizing the influence of the light-induced field. For $a, b, c \to 0$ we return to Eq. (10). As follows from the structure of Eq. (17), the peak value of ρ cannot exceed c^{-1}. The main effect of the trap saturation is thus lowering of the concentration peak. Most probably, this effect becomes weaker outside our simple model, when the photoexcited electrons are allowed to recombine first to numerous intermediate levels.[28] It is clear, anyhow, that the case $a, b, c \ll 1$ is of prime interest for the cleaning purposes.

Importantly, the quasilinear partial differential Eq. (16) can also be effectively solved by the method of characteristics.[17,18] The calculation procedure is reduced here to solving of the set of ordinary differential equations

$$\frac{d\hat{z}}{d\hat{t}} = u(\hat{z}, \rho), \quad \frac{d\rho}{d\hat{t}} = g(\hat{z}, \rho), \tag{19}$$

with the initial conditions $\hat{z}(0) = \xi$ and $\rho(0) = 1$. It gives a family of characteristics $\hat{z} = \hat{z}(\xi, \hat{t})$ and $\rho = \rho(\xi, \hat{t})$ in the 3D space of $\hat{z}$, $\hat{t}$, and ρ. Different values of ξ correspond again to different characteristics. In terms of $\hat{z}$ and $\hat{t}$, the necessary solution for the normalized electron concentration is $\rho(\xi(\hat{z}, \hat{t}), \hat{t})$.

The general outcome of our calculations is simple: For any combination of the small input parameters a, b, and c and for any velocity ratio v/v_0 within the interval [0,1], the spatial profile $\rho(\hat{z})$ breaks and becomes three-valued, i.e., nonphysical, in the close vicinity of the peak for a sufficiently large value of the normalized time $\hat{t}$. The moment of breaking corresponds to the earliest intersection of two characteristics that correspond to two different values of ξ. The region of ambiguity expands gradually with further increasing $\hat{t}$. In the region $\rho(\hat{z}, \hat{t}) \lesssim 1$, which includes the cleaned region, the influence of the field is very weak for $a, b, c \ll 1$. The described behavior is illustrated by line 2 in Fig. 5 plotted for $t/t_0 = 10$, $v/v_0 = 0.6$, and $a = b = c = 0.1$. The multivalued region extends here approximately from −0.75 to 0.68 and the maximum value of ρ is much smaller than for line 1.

Variations in the small parameters a, b, and c change only quantitative details of the behavior of $N_e(\hat{z})/N_e^0$ in the cleaned region. This is illustrated by Fig. 9 which shows quantitatively the negative influence of the parameter a on the ratio N_e^{min}/N_e^0. An increase in a up to 0.3–0.4 does not produce significant changes. However, further increasing results in a steep growth of this ratio and, correspondingly, in a strong deterioration of the cleaning process. The effect of the parameter b on the ratio N_e^{min}/N_e^0 is similar.

The phenomenon of profile breaking is typical for many physical systems obeying quasilinear first-order partial equations, including waves on water surfaces, sound waves, etc.[17,18] Usually, small diffusion-like terms with higher spatial derivatives prevent the breaking, determine the position

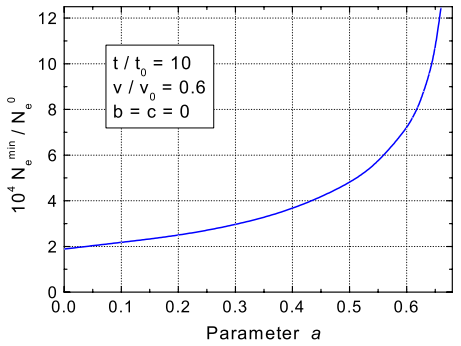

FIG. 9. (Color online) Dependence of the ratio $\rho_{min}=N_e^{min}/N_e^0$ on the dimensionless parameter $a=\sigma_{ph}^0/\sigma_i^0$ for $t/t_0=10$, $v/v_0=0.6$, and $b=c=0$.

and width of a narrow quasidiscontinuity (of the shock-wave front), and remain negligible outside the front. The method of characteristics fails in this case, but more sophisticated calculations show that the front position lies within the region of ambiguity determined by this method.

In the actual case of optical cleaning, we can expect that keeping the weak diffusion terms in Eqs. (1) and (3) will determine the position of the quasidiscontinuity. The main question is here how deep is this position in the cleaned region.

To resolve the problem of ambiguity and to check our expectations, we have modeled directly Eqs. (4)–(6) keeping the diffusion term in the expression (1) for j_e. Line 3 in Fig. 5 shows the corresponding result for $t/t_0=10$, $v/v_0=0.6$, and $a=b=c=0.01$. The quasidiscontinuity is situated at $(z-vt)/z_0\simeq 0.4$; it is inside of the ambiguity region and on the periphery of the cleaned region. The profile of $\rho(\hat{z})$ remains practically unchanged to the left of the quasidiscontinuity, while the shape of the peak to the right of it experiences considerable quantitative changes. The negative influence of the light-induced field on the cleaning process remains thus of minor importance for $a,b,c\ll 1$.

The use of asymmetric moving light beams, as described in Sec. IV A, allows to diminish further the negative influence of the light-induced fields. First, the effect of profile breaking becomes less pronounced in this case because of the broadening of the concentration peak. Second, the cleaned area becomes well separated from the peak in this case.

V. DISCUSSION OF MODEL PREDICTIONS

The most important theoretical prediction is a strong enhancement of the cleaning rate using moving light beams. The decrease of N_e^{min} in time occurs here *exponentially* and much faster compared to the case of standing beams. The maximum (in the beam velocity v) cleaning rate occurs at $v\simeq 0.6v_0$ for the Gaussian beam and asymmetric beams with Gaussian-like trailing edges. This rate increases with decreasing the Gaussian width z_0. Furthermore, the use of a moving beam increases the size of the cleaned area, it becomes much larger than z_0 for $t\gg t_0$. The cleaning performance can be additionally improved by employment of asymmetric light beams.

After the cleaning procedure, the electron concentration profile $N_e(z)$ is generally characterized by a deep and broad minimum (the concentration hole) and a relatively narrow peak caused by the bulldozering effect. While the height and width of the peak are sensitive to the choice of small model parameters a, b, and c, the concentration hole is only weakly affected by this choice.

The conditions for the cleaning enhancement impose restrictions on the input parameters such as the beam size and the peak intensity and these restrictions depend on the material parameters of the sample to be cleaned. It is useful therefore to discuss the optimization of the cleaning process, which is done below, applied to the suppression of optical damage in $LiNbO_3$.

Let us formulate quantitatively the goal of the optical cleaning. The suppression of optical damage can be ensured under the condition of a strong charge exhaustion in the working area of the sample. Let w be the size of the beam to be used, which is expected to be considerably smaller than the sizes of the cleaning beam and of the cleaned area. The maximum achievable value of the light-induced field is then $E_{max}\approx ewN_e^{min}/\epsilon\epsilon_0$, and the corresponding index change is $(\delta n)_{max}=rn^3E_{max}/2$, where n and r are the relevant background refractive index and electro-optic coefficient. For most optical applications, the optical damage is suppressed for $\delta n\lesssim 10^{-5}$. By setting $n=2.2$ and $r=30$ pm/V, which is relevant for extraordinarily polarized beams with the strongest optical damage, and $\epsilon=30$, we obtain the estimate

$$wN_e^{min}\lesssim 10^{10}\ \text{cm}^{-2}. \tag{20}$$

For nonlinear-optical applications, such as frequency doubling, the use of focused beams of the size $w\lesssim 100$ μm has no alternative. In this case, the minimum value of the electron concentration, which must be achieved by the optical cleaning, is $N_e^{min}\approx 10^{12}$ cm^{-3}. This is a very low concentration level even for semiconductors. The expected value of the electron concentration in nominally undoped $LiNbO_3$ crystals, which is due to residual iron centers, is $(10^{15}-10^{16})$ cm^{-3}. Thus, reduction in the electron concentration by (3–4) orders of magnitude can be considered as the goal of the optical cleaning. According to our theory, this goal can be achieved.

Nominally undoped crystals, where the background concentration of photoexcitable electrons is already reduced to a minimum, suit indeed best for application of the optical cleaning method. Nevertheless, doped crystals are also of great interest. The spatial profile $N_e(z)$ can be monitored by absorption spectroscopy in this case, which gives a tool to control the cleaning characteristics. In undoped samples, where the light absorption is extremely small, this tool fails.

Using the definitions of Sec. II, we consider next the most important functional dependences for typical $LiNbO_3$ parameters. Setting the absorption cross-section $s=5\times 10^{-18}$ cm^2 for $\lambda\simeq 477$ nm,[22] we write down the useful scaling relations for the photovoltaic-drift time t_0 and velocity v_0, measured in hours and millimeters per hour,

$$t_0[\mathrm{h}] \simeq 0.2[z_0]/[l_{pv}][I_0], \quad v_0[\mathrm{mm/h}] \simeq 0.47[I_0][l_{pv}]. \tag{21}$$

The square brackets on the right-hand sides indicate that z_0, l_{pv}, and I_0 are measured in the units 100 μm, 1 Å, and 100 W/cm^2, respectively. Importantly, the time t_0 scales linearly with z_0. Any diffusion-based cleaning method would give a quadratic scaling with much longer cleaning times.

Setting the ionic activation energy ε_i=1.1 eV, the preexponent D_i^0=0.3 cm^2/s, and T=177 °C, which is within the tolerance range,[20,25,26] we obtain for the most important dimensionless parameter $a=\sigma_{ph}^0/\sigma_i^0$:

$$a \simeq 35b[I_0][\mu_e\tau_e], \tag{22}$$

where, as earlier, $b=N_e^0/N_i^0$, and $\mu_e\tau_e$ has the unit 10^{-13} cm^2/V. The use of 1.2 instead of 1.1 eV for ε_i, which is also within the range of tolerance, would give a number of 440 instead of 35 in this relation.

The scaling relations (21) and (22) allow to identify the problems of the optical cleaning and to get ideas of how to overcome them. On the one hand, the time t_0 must be not too long to make the cleaning process practically useful. This restricts the intensity I_0 from below and the size z_0 from above. On the other hand, the inequality $a \ll 1$, which is necessary for the cleaning enhancement, restricts I_0 from above. These restrictions are not necessarily conflicting with each other. In particular, they are compatible for undoped crystals where $b \lesssim 10^{-3}$. It is unlikely, however, that they can be combined for doped samples with $N_e^0 \gtrsim 10^{17}$ cm^{-3}. High cleaning performance is not expected (and is not necessary) in this case, but demonstration of the principle and verification of the main dependences should be possible.

Most probably, the optimum parameters I_0 and z_0 lie in the ranges (10–100) W/cm^2 and (0.1–1) mm for undoped $LiNbO_3$ crystals. More precise judgements require additional data on l_{pv}, ε_i, N_e^0/N_i^0, and $\mu_e\tau_e$. According to the literature data,[29,30] a further increase of I_0 can result in an increasing photovoltaic constant β (or l_{pv}). Basically, this feature favors the optical cleaning but requires quantitative modifications of the model used.

As we have mentioned, the bulk photovoltaic effect is inherent in numerous pyro- and piezo-electric crystals, and the characteristic photovoltaic length l_{pv} is not relatively large for $LiNbO_3$ crystals. Therefore, the optical cleaning method is not specific for this optical material. The choice of lithium niobate, as an exemplary material, was caused greatly by its practical importance and a relatively good knowledge of the relevant material and photoelectric properties.

VI. EXPERIMENT

The main goal of this section is an experimental demonstration of the expected strong cleaning and comparison of available experimental data with theory.

In our experiments, we used congruent $LiNbO_3$:Fe crystals with the dimensions $x \times y \times z = 1 \times 4 \times 5$ mm^3, $N_\Sigma \simeq 3.6 \times 10^{18}$, and $N_e^0 \simeq 6 \times 10^{16}$ cm^{-3}. The initial H^+ concentration, deduced from absorption measurements at 2870 nm,[27] was $\simeq 2 \times 10^{18}$ cm^{-3}.

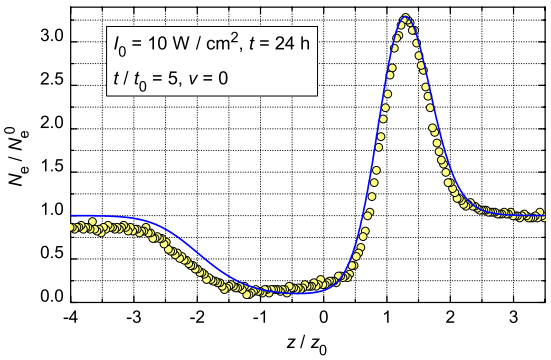

FIG. 10. (Color online) Normalized profile N_e/N_e^0 for $I_0 \approx 10$ W/cm^2 after 24 h cleaning (dots) with a standing light beam (Ref. 15). The solid theoretical line corresponds to a=0.5 and t/t_0=5.

For the cleaning, we employed light beams at 514 and 532 nm from Ar^+ and Nd:YAG lasers, respectively. Each beam was widened and then focused onto the y,z-face using a cylindrical lens with focal length 70 cm. The Gaussian widths used were $z_0 \simeq 70$ μm and 42 μm, respectively. The temperature was kept at 180 °C during the cleaning.

After cooling down to room temperature, inspection of the light-absorption profile was performed in two ways: First, we used a weak light beam at 543 nm with a 1/e-radius of 35 μm from a HeNe laser; moving the crystal yields a scan of the absorption profile with a step of 2.5 μm and hence the profile $N_e(z)$. Second, we used a photospectrometer working at 477 nm with a 100 μm slit aperture placed directly in front of the sample. The crystal was moved relative to the aperture with steps of 50 μm. Because of a larger absorption coefficient, the second method provides a higher sensitivity.

In a first cleaning experiment to be presented, we used the Ar^+ laser. The beam with $I_0 \simeq 10$ W/cm^2 was static (v=0), and the cleaning duration was $t \simeq 24$ h. The resulting concentration profile $N_e(z)$ is well resolved with the HeNe laser, see Fig. 10. A 10-fold reduction in N_e is achieved in the cleaned area.

The solid line in Fig. 10 represents our simulation for t/t_0=5, a=0.5, and $b,c \ll 1$. Good agreement with the experimental results is evident. The smallness of b and c is ensured by the above specified experimental conditions; the effect of these parameters is small. With only two variable parameters remaining, t/t_0 and a, the fitting procedure becomes unambiguous. The found values of these dimensionless parameters correspond to $l_{pv} \simeq 0.4$ Å and $\mu_e\tau_e \simeq 5 \times 10^{-13}$ cm^2/V, respectively, according to Eqs. (21) and (22). These material parameters are within the expected variation range. Note that the simulation includes the convolution of the true profile $\rho(z)$ and the Gaussian profile of the probe beam; this smoothes the peak and decreases N_e^{max} by ≈40%.

In a second experiment, we used more challenging cleaning parameters with a moving Nd:YAG laser beam: $t \simeq 340$ h, $I_0 \simeq 15$ W/cm^2, and $v \simeq 3 \times 10^{-3}$ mm/h, which correspond to $v/v_0 \approx 10^{-1}$, $t/t_0 \approx 10^2$, $a \approx 1$, and $b,c \ll 1$. After the treatment, we were *unable* to resolve light absorption

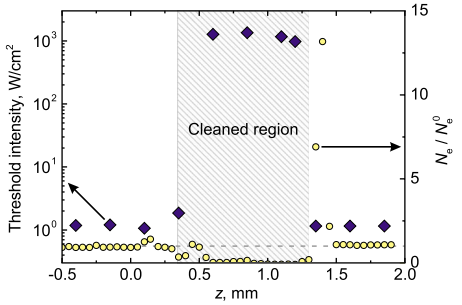

FIG. 11. (Color online) The concentration profile (circles, right scale) and the threshold intensity of optical damage (diamonds, left scale) versus the coordinate z after the long-term cleaning. The errors are given by the heights of the symbols.

in the cleaned ($\approx$1 mm) region using our most sensitive spectometric technique, see Fig. 11. The ratio N_e/N_e^0 has certainly become smaller than the minimum measurable value ($\approx$0.05). At the same time, the peak value of N_e/N_e^0 in front of the cleaned area must be considerably higher than 14 (the highest circle) because the smoothing effect is inevitably strong in the peak area for our absorption measurements. Note that the small bump at $z \approx 0.5$ mm is caused, most probably, by an imperfection of the sample.

Furthermore, a strong reduction of optical damage has been detected after the cleaning.[15] The extent of this reduction can be quantified by measuring the threshold intensity for the onset of optical damage at different positions of the crystal, in untreated regions as well as in the cleaned region: A focused beam (1/e-radius of 20 μm) at 514 nm from an Ar^+ laser was directed onto the sample. After a 10-s-exposure at intensities in the range $(10^{-2}-10^4)$ W/cm^2, the output beam divergence was measured: A microdisk blocked the beam center, so that only the power P_{out} of the stray light was recorded. With the onset of optical damage, P_{out} drastically increased. The light intensity corresponding to this dramatic increase was taken as the threshold intensity. It is increased by more than *three orders of magnitude* in the whole cleaned region with respect to the untreated regions; see Fig. 11.

VII. CONCLUSIONS

A comprehensive and conclusive theory of the optical cleaning is presented. It is based on a general charge-transport model incorporating the bulk photovoltaic effect and the conductivity caused by photoelectrons and thermo-activated ions. It is shown that long-term exposures lead, under proper conditions, to a fast and almost complete removal of photoexcitable electrons from the illuminated area modifying the optical properties of the material.

The theory shows that the effect of optical cleaning is massive: it essentially depends on the variable experimental parameters—the temperature and the intensity, width, shape, and velocity of the cleaning beam—and also on the material parameters, such as the photovoltaic-drift length, the specific photoconductivity, and the concentration of compensating ions. Correspondingly, a wealth of cleaning regimes is available, and a multiparametric optimization of the cleaning performance is an important issue. Properly shaped moving light beams are expected to provide the fastest "exponential cleaning."

The model predictions are supported by cleaning experiments with $LiNbO_3$:Fe crystals showing, in particular, a three orders of magnitude increase in the optical damage threshold.

Surprisingly, the essentials of the method have strong generic links with the known kinetic and hydrodynamic models describing linear and nonlinear waves.

ACKNOWLEDGMENTS

We are grateful to the DFG and the Deutsche Telekom AG for financial support.

[1] V. Fridkin and B. Sturman, *The Photovoltaic and Photorefractive Effects in Noncentrosymmetric Materials* (Gordon and Breach Science Publishers, Philadelphia, 1992).
[2] A. M. Glass, D. von der Linde, and T. J. Negran, Appl. Phys. Lett. **25**, 233 (1974).
[3] Yu. S. Kuzminov, *Lithium Niobate Crystals* (Cambridge International Science Publishing, UK, 1999).
[4] L. E. Myers, R. C. Eckardt, M. M. Fejer, R. L. Byer, W. R. Bosenberg, and J. R. Pierce, J. Opt. Soc. Am. B **12**, 2102 (1995).
[5] N. G. R. Broderick, G. W. Ross, H. L. Offerhaus, D. J. Richardson, and D. C. Hanna, Phys. Rev. Lett. **84**, 4345 (2000).
[6] L. Arizmendi, Phys. Status Solidi **201**, 253 (2004)
[7] K. Buse, Appl. Phys. B: Lasers Opt. **64**, 391 (1997).
[8] L. Solymar, D. Webb, and A. Grunnet-Jepsen, *The Physics and Applications of Photorefractive Materials* (Clarendon Press, Oxford, 1996).
[9] A. Ashkin, G. D. Boyd, J. M. Dziedzic, R. J. Smith, A. A. Ballman, J. J. Levinstein, and K. Nassau, Appl. Phys. Lett. **9**, 72 (1966).
[10] T. Volk, M. Wöhlecke, and N. Rubinina, in *Photorefractive Materials and Their Applications 2*, edited by P. Günter and J.-P. Huignard (Springer, New York, 2007).
[11] Y. S. Bai and R. Kachru, Phys. Rev. Lett. **78**, 2944 (1997).
[12] R. DeSalvo, A. A. Said, D. J. Hagan, E. W. VanStryland, and M. Sheik-Bahae, IEEE J. Quantum Electron. **32**, 1324 (1996).
[13] P. Martin, S. Guizard, Ph. Daguzan, G. Petite, P. D'Oliveira, P. Meynadier, and M. Perdrix, Phys. Rev. B **55**, 5799 (1997).
[14] S. S. Mao, F. Quéré, S. Guizard, X. Mao, R. E. Russo, G. Petite, and P. Martin, Appl. Phys. A: Mater. Sci. Process. **79**, 1695 (2004).
[15] M. Kösters, B. Sturman, P. Werheit, D. Haertle, and K. Buse, Nat. Photonics **3**, 510 (2009).
[16] A. Jeffrey, *Handbook of Mathematical Formulas and Integrals* (Academic Press, New York, 2004).
[17] G. B. Whitham, *Linear and Nonlinear Waves* (Wiley-

Interscience Publications, New York, 1974).
[18] A. Scott, *Nonlinear Science: Emergence and Dynamics of Coherent Structures* (Oxford University Press, Oxford, 2003).
[19] J. J. Amodei and D. L. Staebler, Appl. Phys. Lett. **18**, 540 (1971).
[20] B. I. Sturman, M. Carrascosa, F. Agullo-Lopez, and J. Limeres, Phys. Rev. B **57**, 12792 (1998).
[21] M. Carrascosa, L. Arizmendi, and J. M. Cabrera, in *Photorefractive Materials and Their Applications 1*, edited by P. Günter and J.-P. Huignard (Springer, New York, 2007).
[22] E. Krätzig and O. F. Schirmer, in *Photorefractive Materials and Their Applications I*, edited by P. Günter and J.-P. Huignard, Topics in Applied Physics Vol. 61 (Springer-Verlag, New York, 1988).
[23] H. Kurz, E. Krätzig, W. Keune, H. Engelmann, U. Gonser, B. Dischler, and A. Räuber, Appl. Phys. (Berl.) **12**, 355 (1977).
[24] H. Vormann and E. Krätzig, Solid State Commun. **49**, 843 (1984).
[25] J. M. Cabrera, J. Olivares, M. Carrascosa, J. Rams, R. Müller, and E. Diegues, Adv. Phys. **45**, 349 (1996).
[26] K. Brands, M. Falk, D. Haertle, T. Woike, and K. Buse, Appl. Phys. B: Lasers Opt. **91**, 279 (2008).
[27] S. Klauer, M. Wöhlecke, and S. Kapphan, Phys. Rev. B **45**, 2786 (1992).
[28] B. Sturman, M. Carrascosa, and F. Agullo-Lopez, Phys. Rev. B **78**, 245114 (2008).
[29] F. Jermann and J. Otten, J. Opt. Soc. Am. B **10**, 2085 (1993).
[30] F. Jermann, M. Simon, and E. Krätzig, J. Opt. Soc. Am. B **12**, 2066 (1995).